NKX2-1 regulates cell survival, maturation, and DNA-damage responses as a cofactor of RUNX1 in T-cell acute lymphoblastic leukemia

Linde van Aerschot,[1,2] Sofie Demeyer,[3,4] Kalina Timcheva,[1,2] Elien Heylen,[1,2,5] Paulien Verstraete,[1,2] Dylan De Groote,[1,2] Marino Caruso,[1,2] Lukas Lauwereins,[3,4] Alexandra Veloso,[3,4] Kim R. Kampen,[1,2,6] Daniele Pepe,[1,2] Nancy Boeckx,[7,8] Jonathan Royaert,[1,2] Jelle Verbeeck,[1,2] Heidi Segers,[9,10] Jan Cools,[3,4] Kim De Keersmaecker[1,2#] and David Cabrerizo Granados[1,2#]

[1]Laboratory for Disease Mechanisms in Cancer, Department of Oncology, KU Leuven, Leuven, Belgium; [2]Laboratory for Disease Mechanisms in Cancer, Leuven Cancer Institute (LKI), Leuven, Belgium; [3]Laboratory of Molecular Biology of Leukemia, Department of Human Genetics, KU Leuven, Leuven, Belgium; [4]Laboratory of Molecular Biology of Leukemia, Center for Cancer Biology, VIB, Leuven, Belgium; [5]Centre for Tumour Microenvironment, Barts Cancer Institute, Queen Mary University of London, London, UK; [6]Department of Radiation Oncology (MAASTRO), Maastricht University Medical Center, GROW School for Oncology and Reproduction, Maastricht, the Netherlands; [7]Department of Laboratory Medicine, UZ Leuven, Leuven, Belgium; [8]Laboratory of Experimental Hematology, Department of Oncology, KU Leuven, Leuven, Belgium; [9]Paediatric Haematology and Oncology, University Hospitals Leuven, Leuven, Belgium and [10]Department of Oncology / Pediatric Oncology, KU Leuven, Leuven, Belgium

[#]DCG and KDK contributed equally as senior authors.

Correspondence: D.C. Granados
dcabrerizo-ibis@us.es

K. De Keersmaecker
kim.dekeersmaecker@kuleuven.be

Received: April 8, 2025.
Accepted: December 24, 2025.
Early view: January 8, 2026.

https://doi.org/10.3324/haematol.2025.287966

Abstract

T-cell acute lymphoblastic leukemia (T-ALL) is characterized by ectopic expression of transcription factors, including NKX2-1, which is over-expressed in 5% of patients. NKX2-1 is associated with a cortical immunophenotype and drives metabolic addiction to the serine/glycine synthesis pathway in T-ALL. However, there is still no complete picture of the role of NKX2-1 in T-ALL pathogenesis. We characterized a CRISPR-Cas9 NKX2-1 knockout model of RPMI-8402, the only known T-ALL cell line expressing NKX2-1, and validated the obtained results in patient samples. NKX2-1 knockout caused a less mature immunophenotype and promoted cell cycle progression, in line with the direct transcriptional repression of CDK6 by NKX2-1 that we observed. Furthermore, NKX2-1 protected T-ALL cells from apoptosis and DNA damage. The NKX2-1 protein directly bound DNA repair factors, such as RPA1 and RPA2, and presence of NKX2-1 resulted in differential expression of gene sets related to the repair of DNA damage in RPMI-8402 cells and patient samples. Furthermore, NKX2-1 positive cells showed less induction of DNA damage and apoptosis upon treatment with etoposide, a chemotherapy agent that causes DNA damage that is clinically used to treat T-ALL. Mechanistically, our data supported the hypothesis that RUNX1 is an important co-factor for NKX2-1 transcriptional regulation in T-ALL cells, and that NKX2-1 modulated the composition of RUNX1 protein complexes. Notably, NKX2-1 expressing cells showed higher sensitivity towards RUNX1 inhibition, suggesting a co-operative role in regulating T-ALL cell survival. This work reveals a critical role of NKX2-1 in enhancing T-ALL cell survival by protecting against DNA damage and identifies RUNX1 as an important co-factor in T-ALL pathogenesis.

Introduction

T-cell acute lymphoblastic leukemia (T-ALL) is caused by accumulation of somatic mutations that disrupt differentiation, proliferation, and survival of developing lymphocytes.[1] T-ALL cells typically harbor mutations that inactivate cell cycle regulators, such as CDKN2A/CDKN2B, as well as mutations that hyperactivate the NOTCH1 and PI3K/AKT or IL7R-JAK-STAT signaling pathways. This is often accompanied by alterations in epigenetic factors, such as the EED, EZH2 and SUZ12 proteins of the polycomb repression complex 2 (PRC2), or protein translation factors such as mTOR, CNOT3,

RPL10 or RPL22.[1-4] Furthermore, T-ALL patients can be classified into distinct transcriptional subgroups according to their ectopic expression of a transcription factor such as TAL1, TLX1/3, HOXA, LMO1/2 or NKX2-1.[1]

While significant progress has been made in understanding the pathological processes in various T-ALL subgroups, less is known about the NKX2-1 subgroup.[5] NKX2-1 (also known as NKX2 homeobox 1) is a homeobox transcription factor with a critical role in development of the thyroid, lungs and ventral forebrain.[6] Loss of NKX2-1 expression is associated with pathologies affecting one or more of these organs, such as brain-thyroid-lung syndrome.[7] Moreover, aberrant NKX2-1 expression occurs in several cancer types. In lung adenocarcinoma (LUAD), 12% of patients display *NKX2-1* gene amplifications, with a higher prevalence in EGFR-positive cases where NKX2-1 acts as an oncogene through regulation of ROR1 and LMO3.[8-11] Conversely, NKX2-1 acts as a tumor suppressor in $KRAS^{G12D}$ positive LUAD, resulting in loss of differentiation and enhanced tumor seeding activity by regulating genes implicated in cell-cell organization, like claudin-18.[9,12] NKX2-1 is, therefore, known as a double-edged sword in LUAD, with its function heavily dependent on genetic context. Moreover, NKX2-1 is over-expressed in 16% of neuroendocrine prostate cancers, driving reprogramming of prostate adenocarcinoma into the more aggressive neuroendocrine subtype.[13]

Although NKX2-1 is not expressed during normal T-cell development, ectopic NKX2-1 expression occurs in approximately 5% of T-ALL patients due to chromosomal rearrangements that juxtapose *NKX2-1* to the highly expressed T-cell receptor genes or due to *NKX2-1* gene amplifications. Transcriptional profiling of the NKX2-1 T-ALL subtype has revealed a proliferative gene expression signature, characterized by expression of cell cycle regulatory genes and a CD1a-positive immunophenotype, with cortical developmental arrest similar to the TLX1 subgroup.[5,14] Furthermore, we recently described the transcriptional induction of serine/glycine synthesis enzymes by NKX2-1 in T-ALL and LUAD, which leads to metabolic addiction to the serine/glycine synthesis pathway in NKX2-1-positive tumors.[15] However, understanding of the transcriptional targets of NKX2-1 in T-ALL remains incomplete, and it is still unclear whether NKX2-1 plays additional roles in T-ALL development.

We generated an isogenic RPMI-8402 T-ALL NKX2-1 knockout model to investigate the role of NKX2-1 in T-ALL. We integrated NKX2-1 chromatin immunoprecipitation sequencing (ChIP-seq), RNA-sequencing (RNA-seq), and immunoprecipitation (IP)-mass spectrometry datasets from this cell model and validated our findings in T-ALL patient samples (Figure 1A). Our results demonstrate that NKX2-1 protects cells from apoptosis and DNA damage, conferring a lower sensitivity to etoposide, a chemotherapeutic agent used in clinical practice that causes DNA damage. Additionally, we identify RUNX1 as a co-operative co-factor of NKX2-1 in T-ALL cells, thereby shedding light on the role of NKX2-1 in T-ALL pathogenesis.

Methods

Ethics

Genetic analysis and engineering of RPMI-8402 cells, as well as experiments on human patient derived xenograft (PDX) samples, were approved by the UZ Leuven ethical committee (S67079; S54608). Written informed consent was obtained from all patients or their parents, according to the Declaration of Helsinki.

CRISPR-Cas9

RPMI-8402 cells were electroporated (6 square wave pulses, 0.1 ms interval, 150 V) with a Cas9/GFP-encoding vector (pX458; Addgene) containing a sgRNA targeting NKX2-1 (5'-AAGATGTCAGACACTGAGAA-3'). After 48 hours (hr) of incubation in RPMI-1640 containing 10% fetal calf serum (FCS), non-essential amino acids (Gibco), and 1 mM sodium pyruvate (Gibco), GFP-positive cells were sorted (BD FACS Aria III) and grown to single-cell derived colonies in ClonaCell-TCS (Stemcell Technologies), followed by expansion in liquid cultures in RPMI-1640 with 10% FCS. NKX2-1 knockout efficiency was evaluated by Synthego ICE analysis (v3.0) on Sanger sequencing results from genomic DNA of the targeted NKX2-1 locus.

RNA-sequencing

Total RNA was extracted from RPMI-8402 cells with the RNeasy kit (Qiagen) and was converted to 3' mRNA libraries with the QuantSeq library prep kit (Lexogen). Single-end, 50 bp reads were obtained on an Illumina HiSeq4000. RNA-seq data from T-ALL patients have been previously described.[16] The 40 samples with the highest *NKX2-1* expression from the NKX2-1 subgroup were included for analysis and compared to 40 random samples with no *NKX2-1* expression from the TAL1 subgroup. Reads were mapped to the GENCODE human reference genome (GRCh38, v44) with STAR-aligner (v2.7.11a) and further processed using SAMtools (v1.18). Read counts per gene were obtained with FeatureCounts (Subread v2.0.3). Differential expression analysis was performed with the Limma R-package (v3.50.3) after removing genes with low expression using the FilterByExpression function in EdgeR (v3.36.0). Gene Set Enrichment Analysis (GSEA) was performed on ranked gene lists (GSEA v4.3.2, Broad Institute) with the ranking score calculated as -sign(log2 fold change)*log(adj. *P* value).[17,18] We conducted separate GSEA for each database (KEGG, Reactome, Hallmarks, Gene Ontology). From these results, the final plots in our manuscript were obtained by performing a final GSEA on the pathways with the strongest enrichment. The regulatory network was generated using iRegulon (v1.3) in Cytoscape (v3.8.2) on the significantly differentially expressed genes. Data were analyzed and visualized using RStudio (R v4.1.0).

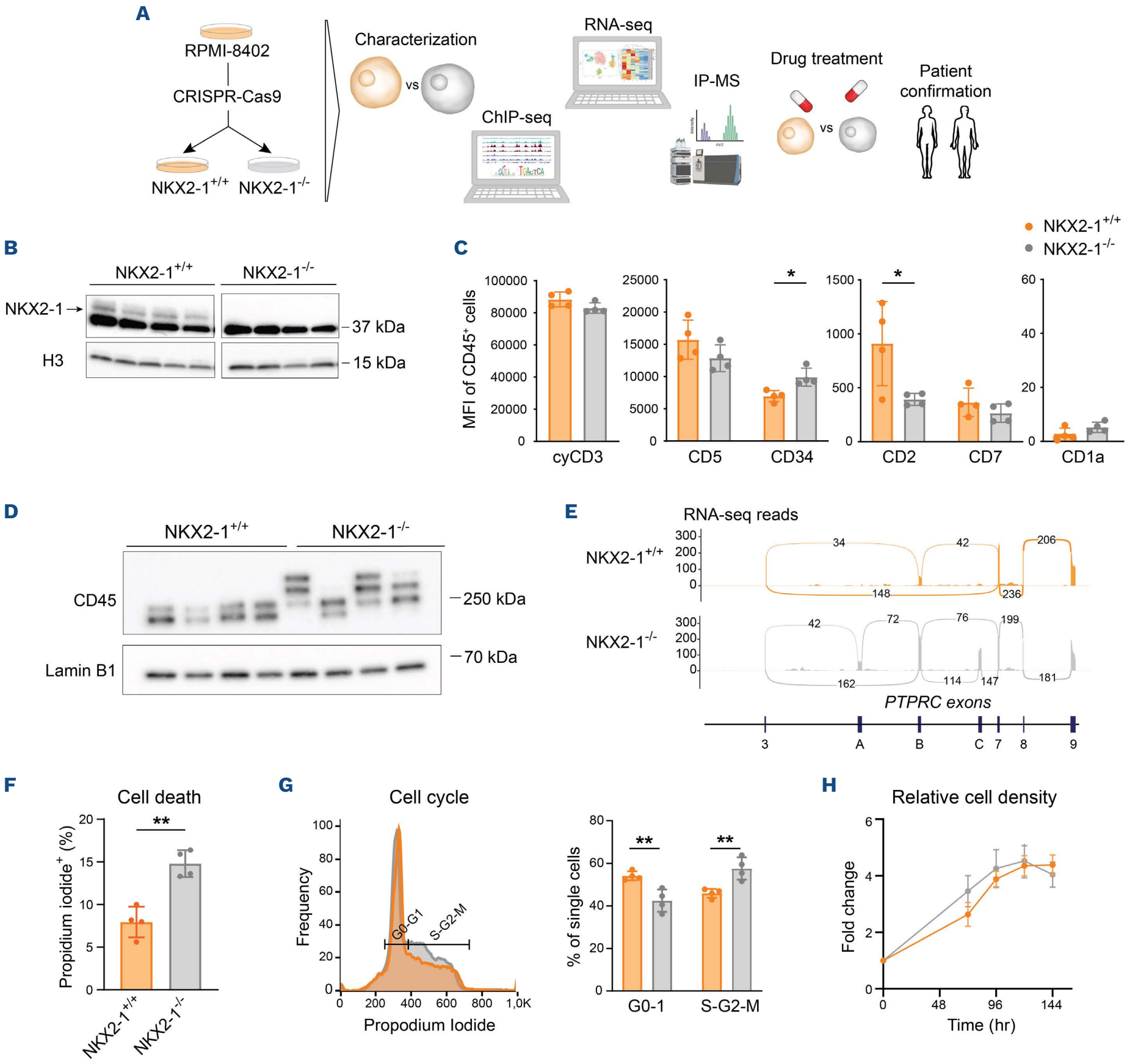

Figure 1. Phenotypic characterization of NKX2-1 in RPMI-8402 cells. (A) Schematic workflow of the study illustrating the NKX2-1 RPMI-8402 knockout model generation, the experiments performed on this model, and confirmation in patient samples. (B) Immunoblot analysis of NKX2-1 in NKX2-1$^{+/+}$ and NKX2-1$^{-/-}$ CRISPR-Cas9 clones used in this project. The NKX2-1 specific signal is indicated with an arrow. The band at 37 kDa is a non-specific signal. Histone 3 (H3) served as loading control. (C) Mean fluorescence intensity (MFI) quantification of CD45^{+} cells based on flow cytometry data of cyCD3, CD5, CD34, CD2, CD7 and CD1a. Data are represented as mean ± Standard Deviation (SD) of 4 clones per genotype. Dots indicate values obtained from individual clones. Statistics were calculated by an unpaired two-tailed *t* test. (D) Immunoblot analysis of CD45 in NKX2-1$^{+/+}$ and NKX2-1$^{-/-}$ RPMI-8402 clones. Lamin B1 served as loading control. (E) Sashimi plot based on RNA-sequencing (RNA-seq) data illustrating differential splicing of *PTPRC* with exon skipping in NKX2-1$^{-/-}$ RPMI-8402 clones. The plot shows data from one representative clone per genotype. A threshold of minimum 20 junction reads was applied. (F) Percentage of propidium iodide (PI)-positive cells detected by flow cytometry in NKX2-1$^{+/+}$ and NKX2-1$^{-/-}$ RPMI-8402 clones at day 5. Data are represented as mean ± SD of 4 clones per genotype. Dots indicate values obtained from individual clones. Statistics were calculated by an unpaired two-tailed *t* test. (G) (Left) Representative cell cycle profiles of NKX2-1$^{+/+}$ and NKX2-1$^{-/-}$ RPMI-8402 clones using PI staining in flow cytometry. (Right) Quantification of G0-G1 and S-G2-M phases at day 5. Data are represented as mean ± SD of 4 clones per genotype. Dots indicate values obtained from individual clones. Statistics were calculated by an unpaired two-tailed *t* test. (H) Proliferation curve of NKX2-1$^{+/+}$ and NKX2-1$^{-/-}$ RPMI-8402 clones. The plotted relative viable cell numbers were determined by PI flow cytometry. Data are represented as mean ± SD of 4 clones per genotype. hr: hours. *P<0.05, **P<0.01.

Sashimi plots were generated using ggsashimi v. 1.1.5.[19]

Immunoprecipitation

Protein extract from each RPMI-8402 NKX2-1$^{+/+}$ and NKX2-1$^{-/-}$ clone, or from PDX-XB14, was used for immunoprecipitation in cell lysis buffer (CST, #9803) supplemented with 5 mM Na_3VO_4 and cOmplete protease inhibitor (Roche). After pre-clearing BSA-blocked Protein G Magnetic Beads (Thermo Fisher Scientific, #88847) with rabbit IgG (CST, #2729), immunoprecipitation was carried out using 1 µg of NKX2-1 (Abcam, #ab67820), 1 µg (for IP) or 5 µg (for IP-MS) of RUNX1 (Thermo Fisher Scientific, #PA-19638), 50-fold dilution of RPA1 (Cell Signaling Technology, #2267) or 0.5, 1 or 5 µg IgG (CST, #2729) antibody. Samples were eluted in Novex Tris-Glycine SDS buffer supplemented with 5% β-mercaptoethanol, followed by western blotting or mass spectrometry analysis.

Statistical analysis

Statistical analyses were performed in GraphPad Prism 10 using the statistical tests indicated in the figure legends. Additional information on the methods used is available in the *Online Supplementary Appendix*.

Results

NKX2-1 promotes maturation and protects T-cell acute lymphoblastic leukemia cells from cell death and cell cycle progression

To identify a relevant model to investigate the role of NKX2-1 in T-ALL, we analyzed NKX2-1 mRNA and protein expression in a panel of 18 human T-ALL cell lines. Because RPMI-8402 was the only cell line expressing NKX2-1 (*Online Supplementary Figure S1*),[20,21] these cells were CRISPR-Cas9 genome edited to generate isogenic NKX2-1 knockout cells (Figure 1A). Four single-cell-derived RPMI-8402 knockout clones, in which no residual NKX2-1 protein was detected on western blot, were chosen, along with four single-cell-derived wild-type control clones (further referred to as NKX2-1$^{-/-}$ and NKX2-1$^{+/+}$ clones, respectively) (Figure 1B).

To characterize the phenotype of knocking out NKX2-1 in RPMI-8402 cells, we first verified the immunophenotype of the obtained NKX2-1$^{+/+}$ and NKX2-1$^{-/-}$ clones. All clones were cyCD3^{+}/CD34^{+}/CD1a^{-}/CD5^{+}/CD7^{low}/CD2^{low} (*Online Supplementary Figure S2A*), consistent with the described RPMI-8402 immunophenotype.[22] Remarkably, NKX2-1$^{+/+}$ clones showed a significant increase in CD2 and a decrease in CD34 mean fluorescence intensity, without altering the percentage of positive cells (Figure 1C). Moreover, whereas total CD45 levels were not affected by NKX2-1 knockout, NKX2-1$^{+/+}$ clones showed expression of lower molecular weight CD45 isoforms due to exon skipping (Figure 1D, E, *Online Supplementary Figure S2B-D*). These isoforms are a marker of T-cell differentiation status,[23] and further underscore the more differentiated T-cell phenotype in NKX2-1$^{+/+}$ cells.[24] NKX2-1$^{+/+}$ clones displayed significantly less apoptotic cell death compared to NKX2-1$^{-/-}$ clones, as assessed by propidium iodide (PI), Annexin V, and cleaved caspase 3 staining (Figure 1F, *Online Supplementary Figure S3*). Interestingly, NKX2-1$^{+/+}$ clones also exhibited a higher percentage of cells in the G0-G1, and a lower percentage in the S-G2-M phases of the cell cycle (Figure 1G). Overall, these apoptosis and cell cycle phenotypes resulted in similar cell densities for NKX2-1$^{+/+}$ and NKX2-1$^{-/-}$ clones over consecutive days (Figure 1H). Collectively, these findings suggest that NKX2-1 promotes a slightly more mature immunophenotype, while also reducing apoptotic cell death and cell cycle progression in RPMI-8402 cells.

NKX2-1 is a transcriptional regulator of CDK6

To investigate the mechanistic role of NKX2-1, we performed NKX2-1 ChIP-seq on NKX2-1$^{+/+}$ clones, with NKX2-1$^{-/-}$ clones as negative controls. The majority of the 496 identified NKX2-1 binding peaks were located in intronic and distal intergenic regions, whereas 21% of the peaks were in promoter regions (Figure 2A, *Online Supplementary Table S1*). Interestingly, we identified 25 genes with an adjacent NKX2-1 ChIP peak that were differentially expressed in RNA-seq on NKX2-1$^{+/+}$ *versus* NKX2-1$^{-/-}$ RPMI-8402 clones (*Online Supplementary Figure S4*). Among the genes with NKX2-1 peaks, cyclin dependent kinase 6 (*CDK6*) was identified, essential for the progression from G1 to S phase in the cell cycle.[25] Furthermore, an open chromatin and enhancer region was observed in the same intronic area in public ATAC-seq and H3K27ac ChIP-seq data from RPMI-8402 cells, as well as a RUNX1 binding site (Figure 2B). Dual luciferase reporter assays in HEK-293T cells showed that NKX2-1 and RUNX1 are co-operatively regulating the activity of this *CDK6* enhancer region (*Online Supplementary Figure S5*). Interestingly, CDK6 mRNA and protein levels were significantly reduced in NKX2-1$^{+/+}$ compared to NKX2-1$^{-/-}$ RPMI-8402 clones (Figure 2C-E). Altogether, these results support the hypothesis that NKX2-1 acts as a transcriptional regulator of CDK6, which is in line with the impaired cell cycle progression that we observed in NKX2-1$^{+/+}$ cells.

RNA-sequencing of NKX2-1 RPMI-8402 model reveals three clusters of differentially expressed gene sets

To further explore the role of NKX2-1 in T-ALL, we characterized the downstream effects of NKX2-1 by performing RNA-seq on our NKX2-1$^{+/+}$ *versus* NKX2-1$^{-/-}$ RPMI-8402 clones. Principal component analysis showed that the two analyzed genotypes formed separate clusters, and we identified 96 significantly differentially expressed genes (DEG) (Figure 3A, *Online Supplementary Figure S6*). Using GSEA, we confirmed enrichment of cell cycle-related pathways in the down-regulated genes in NKX2-1$^{+/+}$ clones (Figure 3B). This GSEA revealed three additional major groups of gene sets regulated by NKX2-1, which were related to ribosome

biology, epigenetics and DNA damage (Figure 3C, *Online Supplementary Figure S7A*). As follow-up of these findings on ribosomal gene sets, we compared the functionality of ribosomes in NKX2-1$^{+/+}$ and NKX2-1$^{-/-}$ RPMI-8402 clones. However, no significant differences were observed in ribosomal polysome profiles or nascent protein synthesis levels (*Online Supplementary Figure S7B-D*), suggesting that NKX2-1 does not substantially affect ribosomal function.

To further investigate the epigenetic gene set cluster identified in the GSEA (Figure 3C), we performed western blot analysis of several histone marks to examine the impact of NKX2-1 expression on the overall epigenetic landscape. NKX2-1$^{+/+}$ clones exhibited lower levels of H3K27ac, a marker of active chromatin, as well as reduced levels of H3K4me1 and H3K4me3, markers of active promoters and enhancers, respectively (Figure 3D). We hypothesized that the reduced histone mark levels in NKX2-1$^{+/+}$ clones may cause differential sensitivity to epigenetic drugs such as HDAC inhibitors (HDACi). Indeed, we observed a significantly decreased sensitivity of the NKX2-1$^{+/+}$ clones against the HDACi romidepsin and vorinostat (Figure 3E). This trend was confirmed in *ex vivo* cultured PDX samples exposed to romidepsin treatment, showing lower sensitivity on NKX2-1 positive samples (Figure 3F, *Online Supplementary Figure S8*). Therefore, we concluded that NKX2-1 reduces the levels of histone modifications in T-ALL, making the cells resistant to HDACi.

NKX2-1 protects T-cell acute lymphoblastic leukemia cells from DNA damage

Interestingly, DNA damage was also identified as a key cluster of differentially expressed gene sets in NKX2-1$^{+/+}$ *versus* NKX2-1$^{-/-}$ RPMI-8402 clones (Figure 3C). This led us to hypothesize that NKX2-1 may protect cells from DNA damage in T-ALL. To investigate this, we assessed the DNA damage status of the NKX2-1$^{+/+}$ and NKX2-1$^{-/-}$ clones by analyzing the γ-H2AX levels, a marker of DNA double strand breaks. NKX2-1$^{+/+}$ clones had significantly lower γ-H2AX levels compared to the NKX2-1$^{-/-}$ clones (Figure 4A). Additionally, we measured DNA damage markers H3K27me3, H3K56ac and H4K20me3 levels, and we observed the same reduction as for γ-H2AX in the NKX2-1$^{+/+}$ clones (Figure 4A). Since induction of DNA damage is often used as a therapeu-

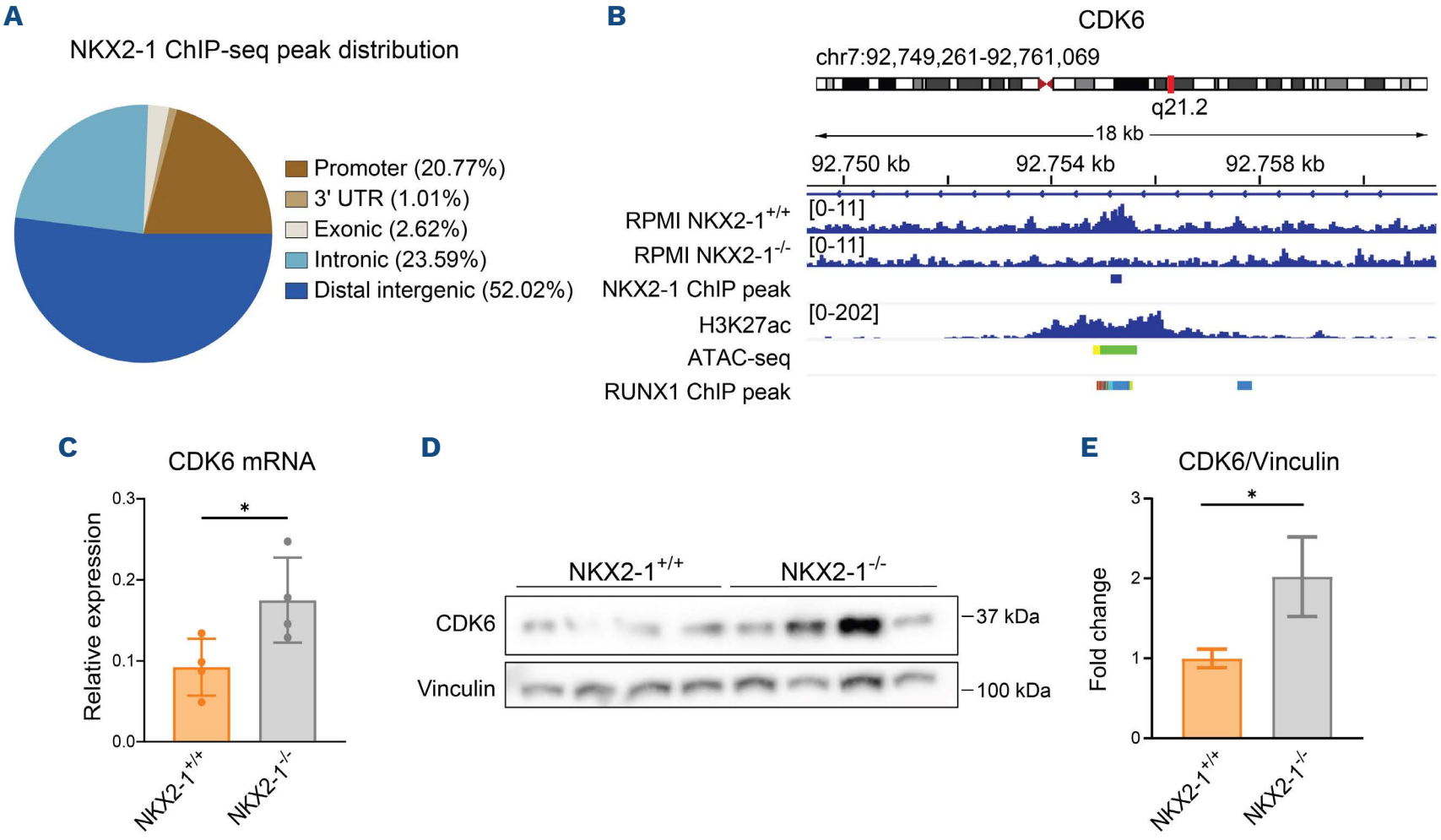

Figure 2. NKX2-1 directly represses CDK6 expression. (A) Peak distribution of NKX2-1 chromatin immunoprecipitation-sequencing (ChIP-seq) in NKX2-1$^{+/+}$ RPMI-8402 cells as defined by ChIPseeker. (B) Genomic locus of the *CDK6* gene with NKX2-1 ChIP-seq peak, H3K27ac ChIP-seq and ATAC-seq signal in RPMI-8402 cells, and RUNX1 ChIP-seq peaks from 22 hematopoietic cell models obtained from chip-atlas.org. (C) Quantification of CDK6 mRNA expression by real-time quantitative polymerase chain reaction (RT-qPCR) in NKX2-1$^{+/+}$ and NKX2-1$^{-/-}$ RPMI-8402 clones at day 5. Individual dots represent 4 biologically independent clones per genotype. Data are represented as mean ± Standard Deviation Statistics were calculated by an unpaired two-tailed *t* test. (D) Immunoblot analysis of CDK6 in the NKX2-1$^{+/+}$ and NKX2-1$^{-/-}$ RPMI-8402 clones. Vinculin served as loading control. (E) Fold change of CDK6 protein expression densitometry of western blots from 3 independent experiments on NKX2-1$^{+/+}$ and NKX2-1$^{-/-}$ RPMI-8402 clones at day 5. Data are represented as mean ± Standard Error of Mean. Statistics were calculated by two-way ANOVA. *P<0.05.

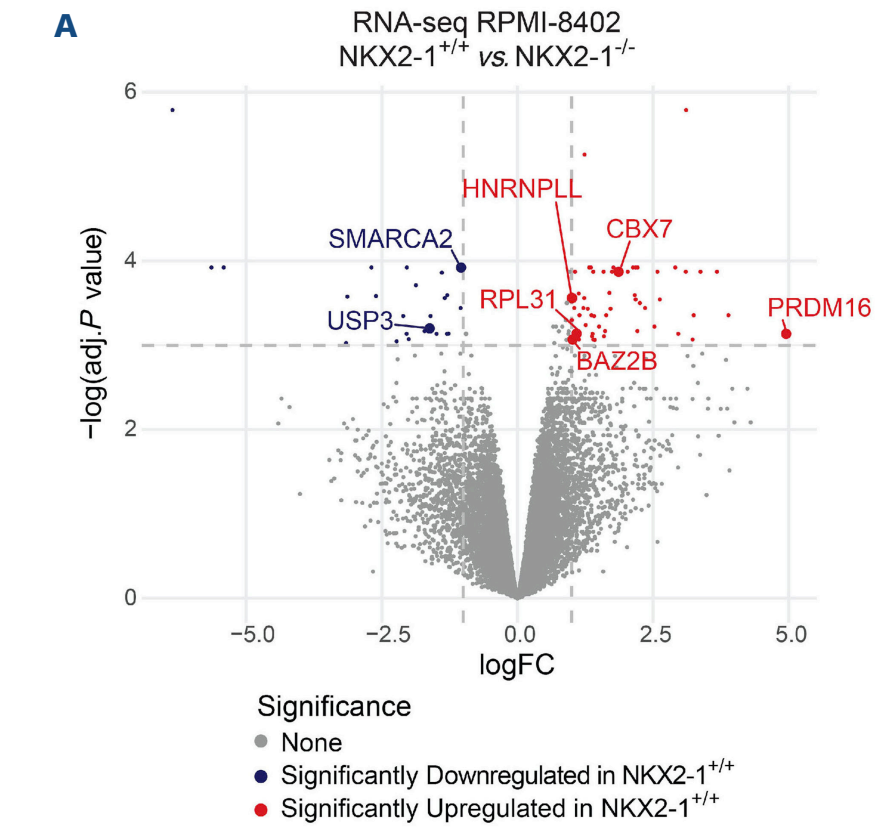

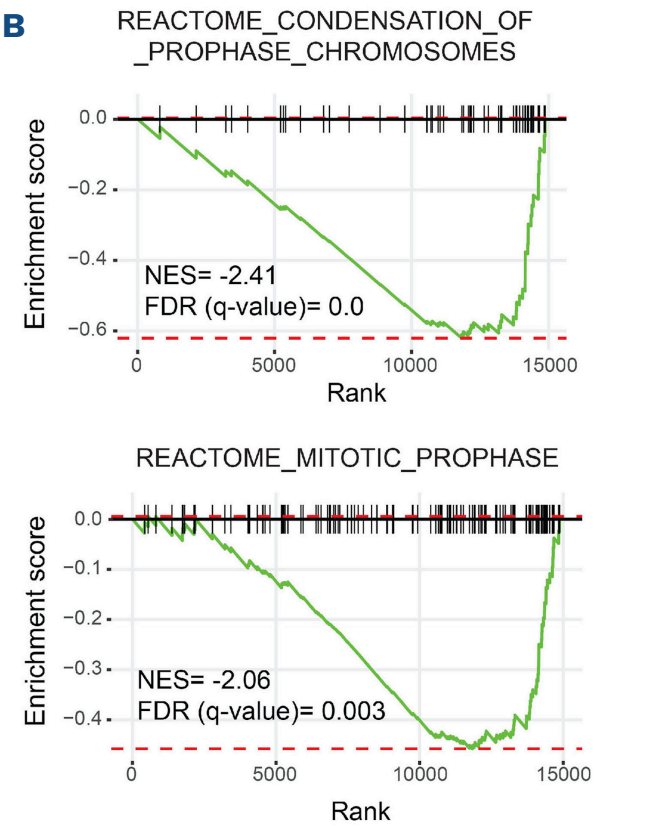

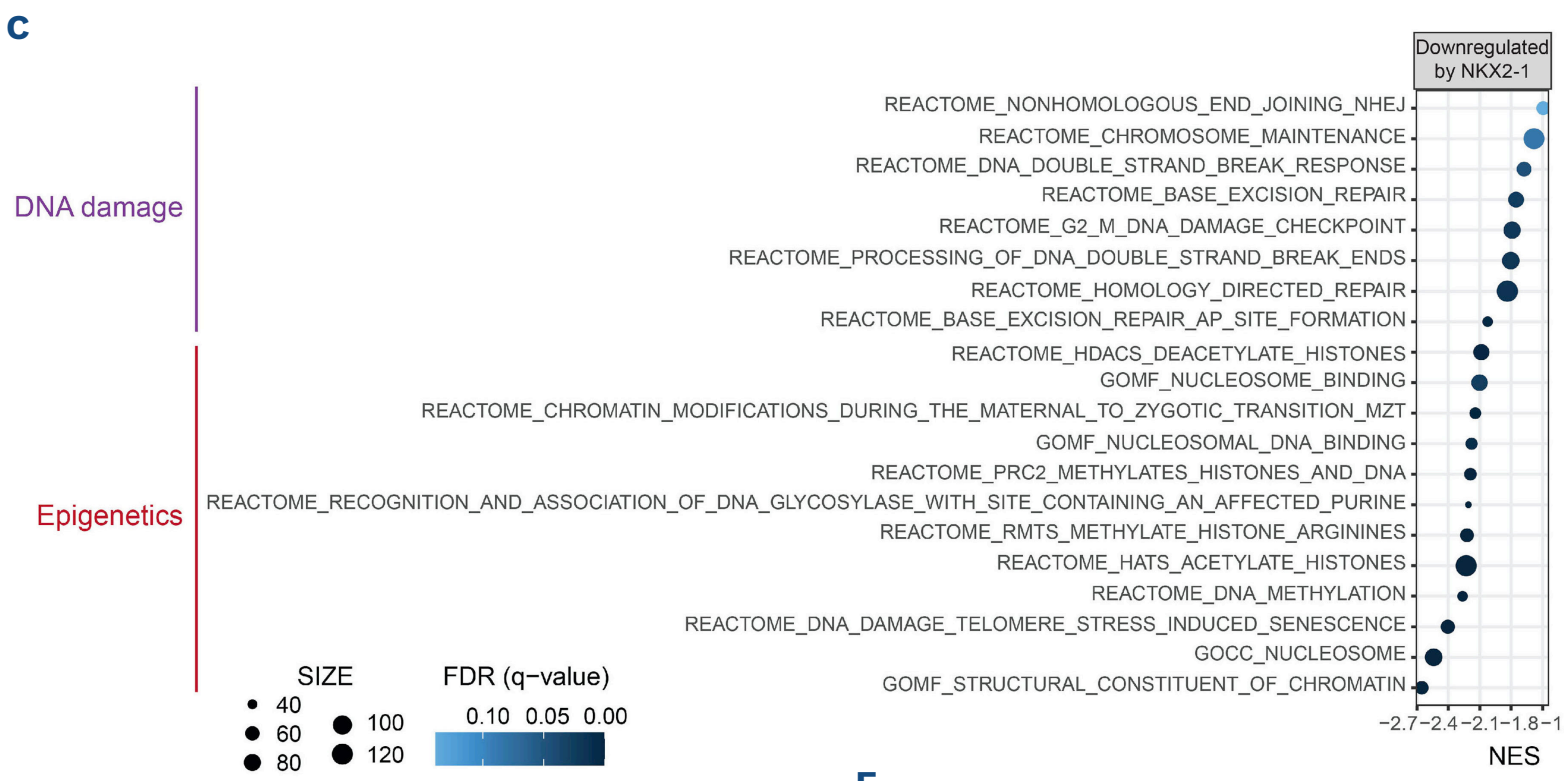

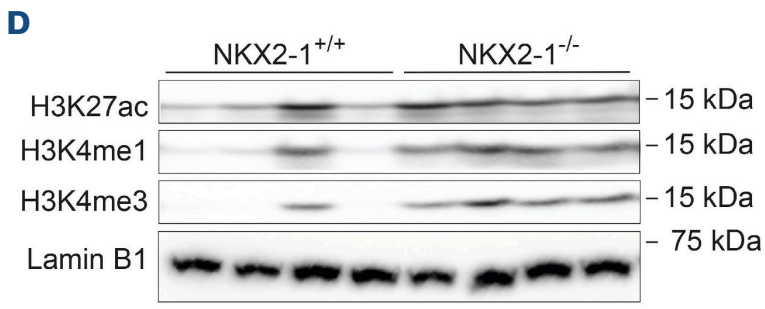

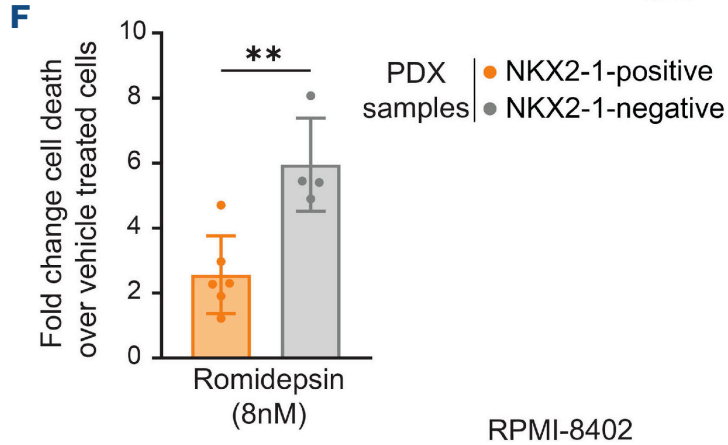

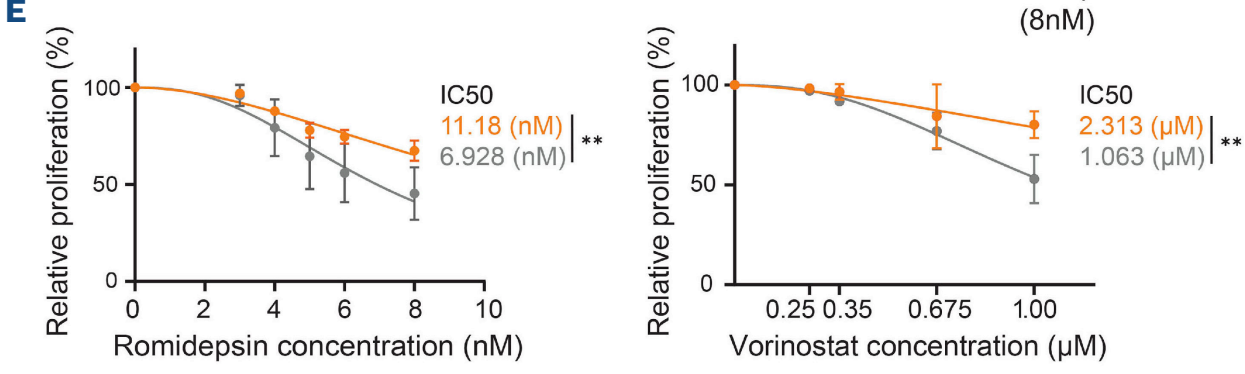

Continued on following page.

Figure 3. RNA-sequencing of NKX2-1$^{+/+}$ and NKX2-1$^{-/-}$ RPMI-8402 clones reveals differentially expressed gene sets related to DNA damage and epigenetics, altering the epigenetic landscape and sensitivity towards HDAC inhibitors. (A) Volcano plot showing differentially expressed genes detected by RNA-sequencing (RNA-seq) analysis of NKX2-1$^{+/+}$ and NKX2-1$^{-/-}$ RPMI-8402 clones (4 clones per genotype). The gray dotted lines indicate the cut-off values for significance (adj.*P* value <0.05) and fold change (FC>2). (B) Gene Set Enrichment Analysis (GSEA) plots showing downregulation of cell cycle-related gene sets in NKX2-1$^{+/+}$ RPMI-8402 cells. (C) GSEA dot plot showing the top enriched gene sets belonging to the DNA damage and epigenetic cluster in the NKX2-1$^{+/+}$ RPMI-8402 model. (D) Immunoblots of H3K27ac, H3K4me1 and H3K4me3 in NKX2-1$^{+/+}$ and NKX2-1$^{-/-}$ RPMI-8402 clones. Lamin B1 served as loading control. (E) Dose-response curves of NKX2-1$^{+/+}$ and NKX2-1$^{-/-}$ RPMI-8402 clones treated for 48 hours with romidepsin (left) or vorinostat (right). Data points represent mean ± Standard Deviation (SD) of relative proliferation of 4 biologically independent clones per genotype, normalized to day 0 and DMSO vehicle condition. Least-squares regression fits to the mean are shown (solid lines), and IC_{50} values were determined for each drug and condition. Statistics were calculated by an extra sum-of-squares F-test. (F) Relative cell death of NKX2-1-positive and -negative patient derived xenograft (PDX) samples after treatment for 72 hours with romidepsin. Data were normalized to DMSO vehicle treated cells. Data are represented as mean ± SD. Statistics were calculated by an unpaired two-tailed *t* test. ***P*<0.01.

tic strategy, we examined the impact of NKX2-1 expression on cellular sensitivity to etoposide, a DNA-damaging agent used in clinical practice. As expected, following drug treatment, NKX2-1$^{+/+}$ clones demonstrated higher viability and lower levels of DNA damage markers γ-H2AX, H3K27me3 and olive moment in comet assays (Figure 4B-D, *Online Supplementary Figure S9*). Also, for other clinically used DNA-damaging agents, such as doxorubicin and 6-thioguanine (6-TG), NKX2-1$^{+/+}$ clones showed a significantly higher IC_{50} value as compared to NKX2-1$^{-/-}$ cells (*Online Supplementary Figure S10*). To corroborate these findings in patients, we analyzed public RNA-seq data of T-ALL patients by utilizing the data sets presented by Pölönen *et al.*[16] We selected the 40 samples with the highest NKX2-1 expression (NKX2-1 positive) as well as 40 samples lacking NKX2-1 expression belonging to the TAL1 subgroup (NKX2-1 negative). These TAL1 samples are an ideal control group, since they are not driven by a homeobox transcription factor but immunophenotypically resemble NKX2-1 positive T-ALL (*Online Supplementary Figure S11*).[26] GSEA analysis on the RNA expression profiles of NKX2-1 positive *versus* negative samples revealed up-regulated DNA damage repair pathways in the NKX2-1 positive group (Figure 4E, F, *Online Supplementary Figure S12*). Interestingly, drug treatments on *ex vivo* cultured PDX samples also showed a trend towards more etoposide resistance in NKX2-1 positive samples (Figure 4G, *Online Supplementary Figure S13*). Taken together, these findings support the hypothesis that NKX2-1 serves a protective role against DNA damage in T-ALL cells.

RUNX1 is a co-factor for transcriptional regulation by NKX2-1

To further elucidate the molecular mechanisms underlying NKX2-1 function in T-ALL cells, we identified NKX2-1 binding partners by IP of NKX2-1 in NKX2-1$^{+/+}$ RPMI-8402 cells, followed by MS analysis, using NKX2-1$^{-/-}$ clones and IgG IP-MS as controls. Besides NKX2-1 itself, eight interacting proteins were identified (Figure 5A). Among these interactors, we identified RUNX Family Transcription Factor 1 (RUNX1), a critical hematopoietic transcription factor implicated in T-ALL.[22,27-29] We confirmed binding of NKX2-1 to RUNX1 by co-IP in our RPMI-8402 cell model and in an NKX2-1-positive PDX T-ALL sample (XB14) (Figure 5B, *Online Supplementary Figure S14*).

In addition to the physical interaction between the NKX2-1 and RUNX1 proteins, our data suggested a co-operative role of RUNX1 and NKX2-1 in regulating gene expression in T-ALL. First, we used iRegulon to predict the transcriptional regulators of DEG in the RNA-seq on the NKX2-1 RPMI-8402 cell model, identifying RUNX1 as a major regulator of these transcripts (Figure 5C, *Online Supplementary Figure S15*). Secondly, HOMER motif analysis of our NKX2-1 ChIP-seq data identified RUNX1 as one of the top-scoring motifs, alongside the NKX2 homeobox family (Figure 5D, *Online Supplementary Table S2*). Besides confirming the specificity of our NKX2-1 ChIP-seq, this result suggests RUNX1 co-binding at NKX2-1 genomic binding sites. Finally, iRegulon analysis of public RNA-seq data from T-ALL patients confirmed RUNX1 as a key transcriptional regulator of DEG in NKX2-1 positive *versus* negative samples, with an even higher normalized enrichment score (NES) than NKX2-1 itself (Figure 5E, *Online Supplementary Figure S16*). Moreover, GSEA analysis indicated a significant positive enrichment of the Reactome pathway of RUNX1-regulated genes involved in the differentiation of hematopoietic stem cells (HSC) in NKX2-1-positive patient samples (Figure 5F). Collectively, these data suggest that RUNX1 functions as co-factor of NKX2-1, working in close co-operation in the transcriptional regulation of T-ALL.

NKX2-1 modulates the binding partners of RUNX1 and cellular sensitivity to RUNX1 inhibition

To better understand the mechanistic interplay between NKX2-1 and RUNX1, we investigated the binding partners of RUNX1 in the presence and absence of NKX2-1 by IP-MS in our RPMI-8402 cell clones (*Online Supplementary Figure S17*). When comparing each condition to its corresponding IgG control, the majority (62%; 396/641) of identified RUNX1 binding partners were not affected by NKX2-1 status (Figure 6A). Furthermore, 18% of the RUNX1 protein partners in NKX2-1$^{+/+}$ clones were absent in NKX2-1$^{-/-}$ clones, with NKX2-1 itself being one of them. Conversely, 29% of the RUNX1 protein partners in NKX2-1$^{-/-}$ clones were exclusive

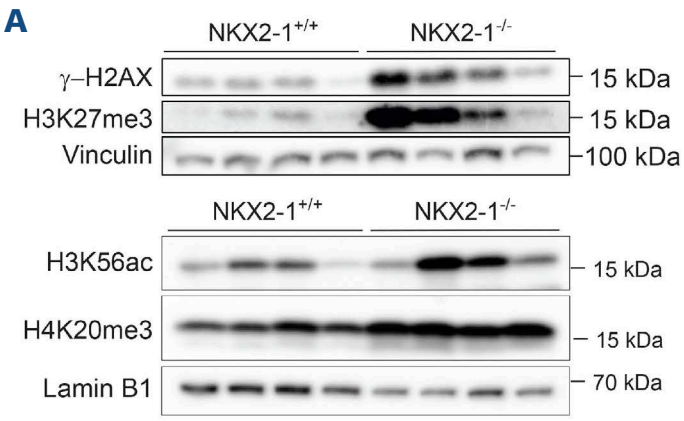

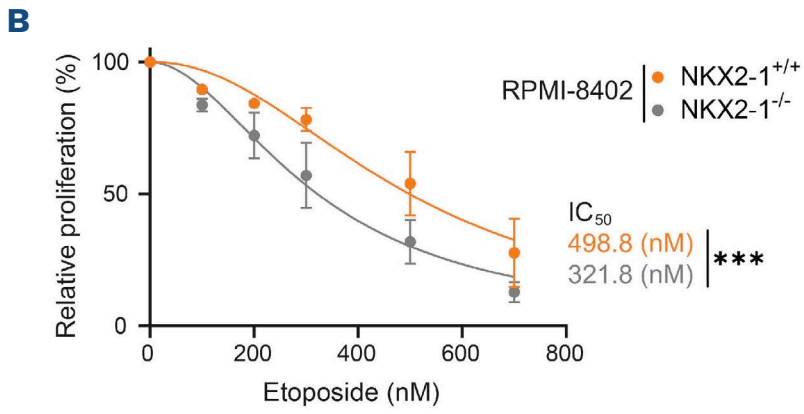

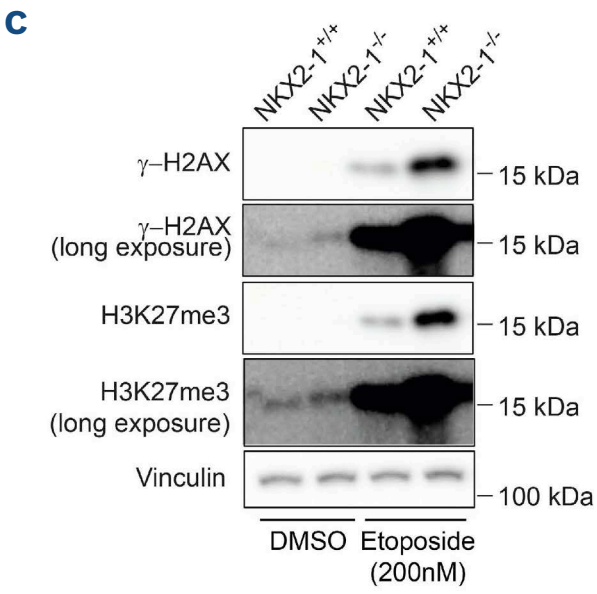

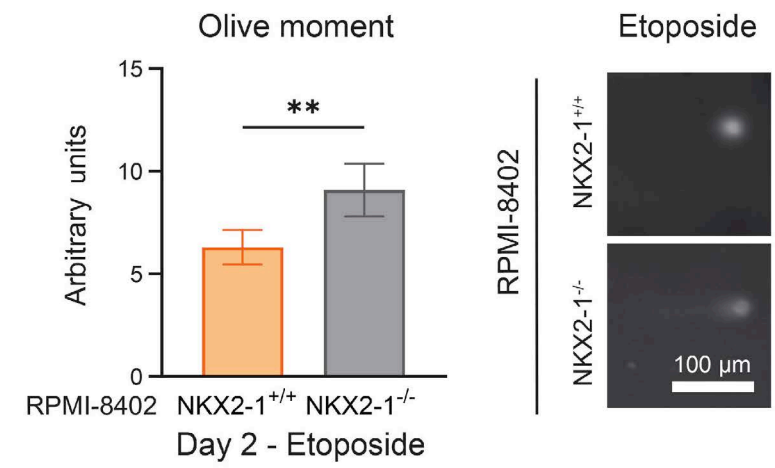

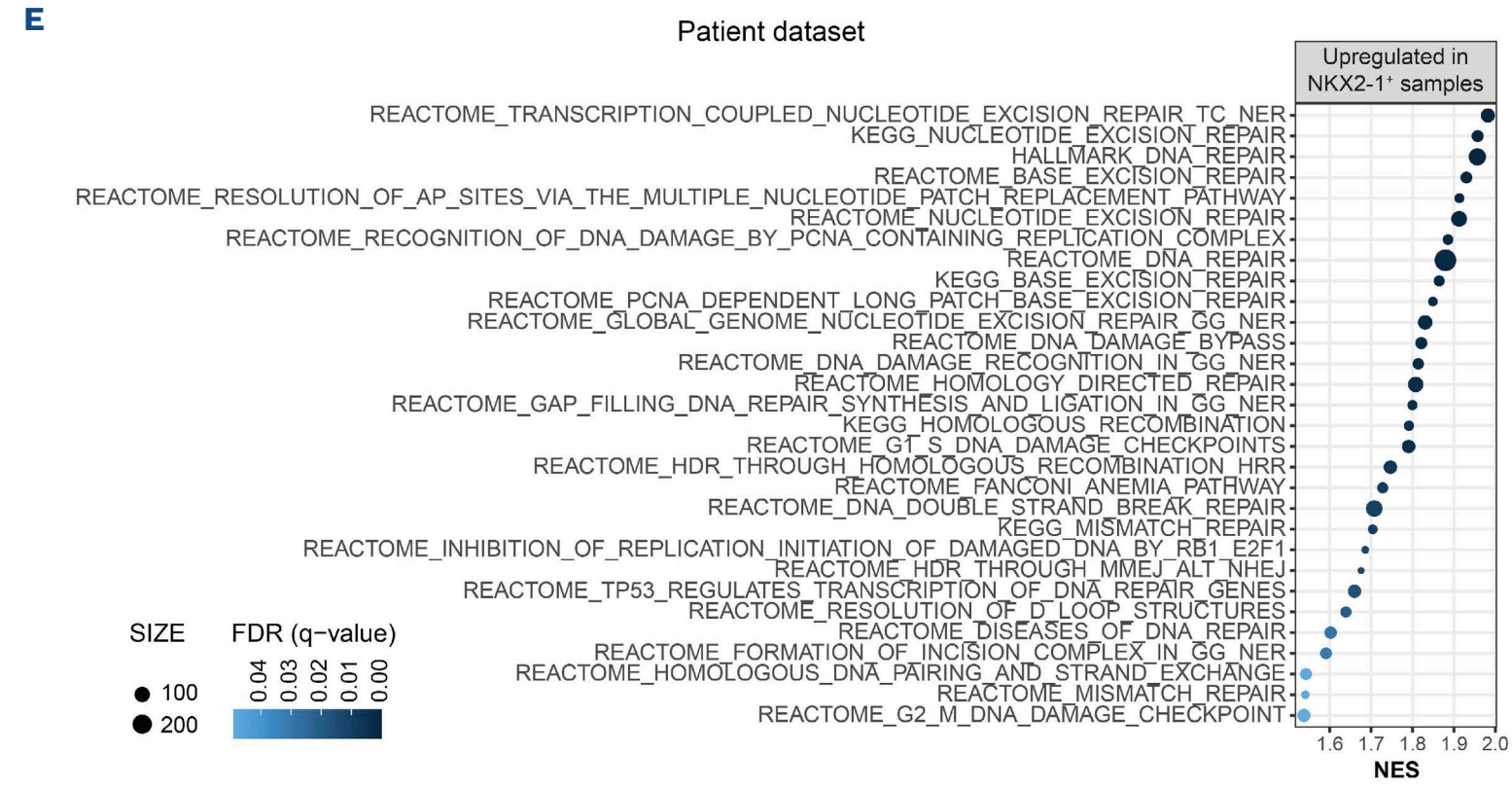

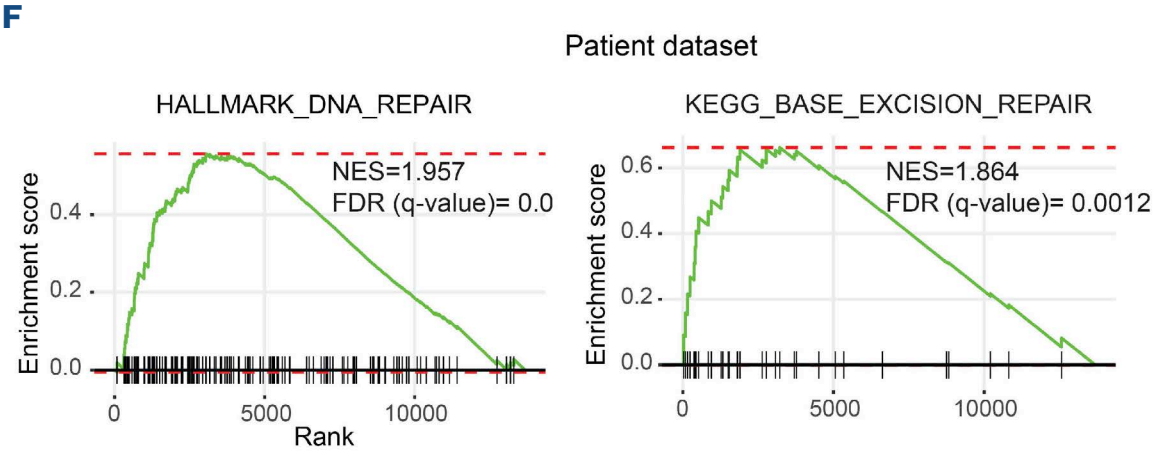

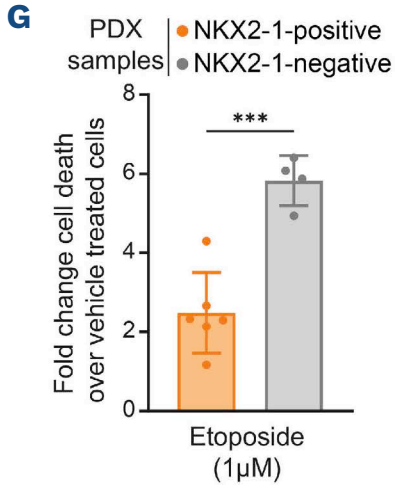

Continued on following page.

Figure 4. NKX2-1 protects cells against DNA damage. (A) (Top) Immunoblot analysis of γ-H2AX and H3K27me3 in NKX2-1$^{+/+}$ and NKX2-1$^{-/-}$ RPMI-8402 clones. Vinculin served as loading control. (Bottom) Immunoblot analysis of H3K56ac and H4K20me3 in NKX2-1$^{+/+}$ and NKX2-1$^{-/-}$ RPMI-8402 clones. Lamin B1 served as loading control. (B) Dose-response curves of NKX2-1$^{+/+}$ and NKX2-1$^{-/-}$ RPMI-8402 clones treated for 48 hours (hr) with etoposide. Data points represent mean ± Standard Deviation (SD) of relative proliferation of 4 clones per genotype, normalized to day 0 and DMSO vehicle condition. Least-squares regression fits to the mean are shown (solid lines), and IC_{50} values were determined. Statistics were calculated by an extra sum-of-squares F-test. (C) Immunoblot for γ-H2AX and H3K27me3 (short and long exposure) in NKX2-1$^{+/+}$ and NKX2-1$^{-/-}$ RPMI-8402 samples (mix of 4 clones per genotype) after treatment with 200 nM etoposide for 48 hr. Vinculin served as loading control. (D) (Left) Olive moment in comet assay on NKX2-1$^{+/+}$ and NKX2-1$^{-/-}$ RPMI-8402 cells after 48 hr of treatment with 200 nM etoposide. Data represented as mean ± Standard Error of Mean (SEM). Statistics were calculated by a Mann-Whitney two-tailed test. (Right) Representative comet stained with propidium iodide (PI) obtained from NKX2-1$^{+/+}$ and NKX2-1$^{-/-}$ RPMI-8402 cells after 48 hr of treatment with 200 nM etoposide. (E) Dot plot showing enriched gene sets linked to DNA damage repair identified in the Gene Set Enrichment Analysis (GSEA) of differentially expressed genes in NKX2-1-positive *versus* negative T-ALL (patient data from Pölönen *et al.*[16]). (F) GSEA enrichment plots showing upregulation of DNA repair gene sets in NKX2-1-positive T-ALL patients. (G) Relative cell death of NKX2-1-positive and -negative patient derived xenograft (PDX) samples after treatment for 72 hr with 1 μM etoposide. Data are normalized to DMSO vehicle treated cells. Data are represented as mean ± SD. Statistics were calculated by an unpaired two-tailed *t* test. ***P*<0.01, ****P*<0.001.

to this condition (Figure 6A). These results suggest that whereas NKX2-1 affects a significant fraction of RUNX1 binding partners, the majority of RUNX1 interactors are insensitive to NKX2-1 presence.

When we compared the obtained RUNX1 interacting proteins to the previously identified NKX2-1 binding partners, we observed that all NKX2-1 interactors also bound RUNX1, except for Thymosin Beta 4 X-Linked (TMSB4X) (Figure 6A). Among these shared binding partners of NKX2-1 and RUNX1, we identified Replication Protein A1 and A2 (RPA1 and RPA2), which are involved in DNA damage recognition and nucleotide excision repair.[30] Given our previous results supporting a role for NKX2-1 in protecting cells from DNA damage, we used co-IP experiments to confirm that RPA1 binds NKX2-1 and RUNX1 in the NKX2-1 RPMI-8402 cell model and in NKX2-1-positive PDX samples (XB14) (*Online Supplementary Figure S18*).

Next, we aimed to evaluate the cellular effects of RUNX1 inhibition. We tried to reduce RUNX1 expression with shRNA. Unfortunately, RUNX1 knockdown was quickly lost in the cells, likely due to its toxicity, preventing us from performing the intended experiments. Therefore, we examined the effects of RUNX1 pharmacological inhibitor Ro5-3335.[31] We assessed our NKX2-1 RPMI-8402 clones over five days and observed a dose-dependent reduction in proliferation and increase in cell death (*Online Supplementary Figure S19A-D*). By day 5, Ro5-3335 exhibited its most significant effect, causing similar levels of cell death at the highest drug concentrations irrespective of NKX2-1 status (Figure 6B). Interestingly, the kinetics of drug response was different at lower drug concentrations: whereas NKX2-1$^{+/+}$ cells started to respond (induction of PI-positive cells) from 2.5 μM of Ro5-3335 upwards, drug-induced cell death only became apparent in NKX2-1$^{-/-}$ cells when a dose of 10 μM Ro5-3335 was applied (Figure 6B). NKX2-1$^{+/+}$ cells were also sensitized to AI-10-47,[32] another pharmacological RUNX1 inhibitor (*Online Supplementary Figure S19E*). This difference in drug sensitivity was also reflected in the accumulation of DNA damage, with NKX2-1$^{+/+}$ cells showing more Ro5-3335-induced DNA damage as compared to NKX2-1$^{-/-}$ cells in comet assays (Figure 6C). Finally, Ro5-3335 was also able to induce apoptosis in *ex vivo* cultured NKX2-1$^{+/+}$ T-ALL PDX samples (Figure 6D, E, *Online Supplementary Figure S20*). Altogether, our results with RUNX1 inhibitor Ro5-3335 support the hypothesis that RUNX1 is essential for survival of T-ALL cells, irrespective of NKX2-1 status. However, the higher relative drug sensitivity of NKX2-1$^{+/+}$ cells, particularly with respect to induction of DNA damage, suggests dependence of NKX2-1 on RUNX1 to execute its role in protecting T-ALL cells from DNA damage and induction of cell death.

Discussion

To better understand the role of NKX2-1 in T-ALL, we developed an isogenic cell model by knocking out NKX2-1 in the RPMI-8402 cell line. We opted for this model instead of over-expressing NKX2-1 in other T-ALL cell lines since their transcriptional programs are driven by other T-ALL-associated transcription factors, potentially confounding the results. Depletion of NKX2-1 in RPMI-8402 cells resulted in a slightly less mature phenotype, as evidenced by the differentiation-associated shifts in CD2 and CD34 expression. These changes suggest that NKX2-1 plays a role in maintaining a more differentiated T-cell state. Consistent with these results, our analysis of public RNA-seq data from T-ALL patients revealed that NKX2-1-positive tumors display upregulation of gene sets linked to HSC differentiation. Further underscoring this role in regulating T-cell differentiation, NKX2-1$^{+/+}$ clones expressed lower molecular weight CD45 isoforms. Interestingly, we found Heterogeneous Nuclear Ribonucleoprotein L Like (*HNRNPLL*), a gene showing NKX2-1 binding in our ChIP-seq, to be up-regulated by NKX2-1 in our RNA-seq results (*Online Supplementary Figure S4*). This gene causes CD45 transcript exon-skipping, in line with our results. In public patient data, we also observed a significant increase of *HNRNPL* (LogFC 0.45, adj.*P* value 0.00016), which has a similar activity as its paralog *HNRNPLL*.[33] We observed that

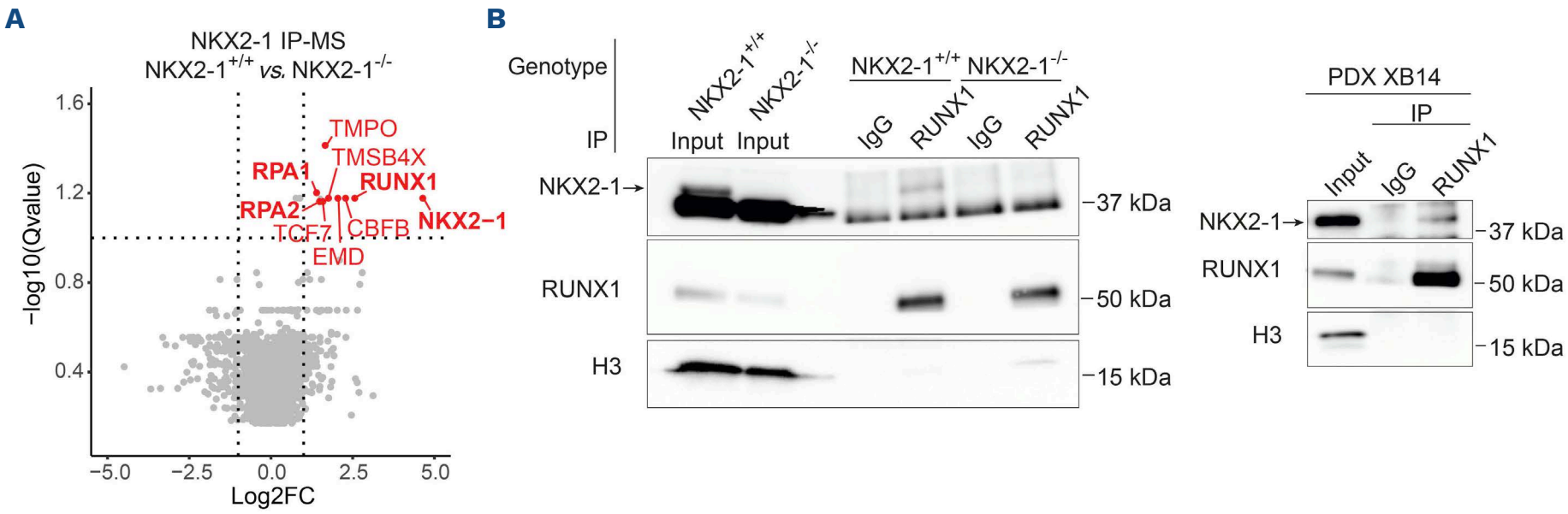

D

HOMER motif analysis on NKX2-1 ChIP-seq

Motifs	Motif scores		
	% of targets	% of background	*P*
RUNX (Runt)	25.40	9.50	1e-23
NKX2-2 (Homeobox)	50.20	30.53	1e-19

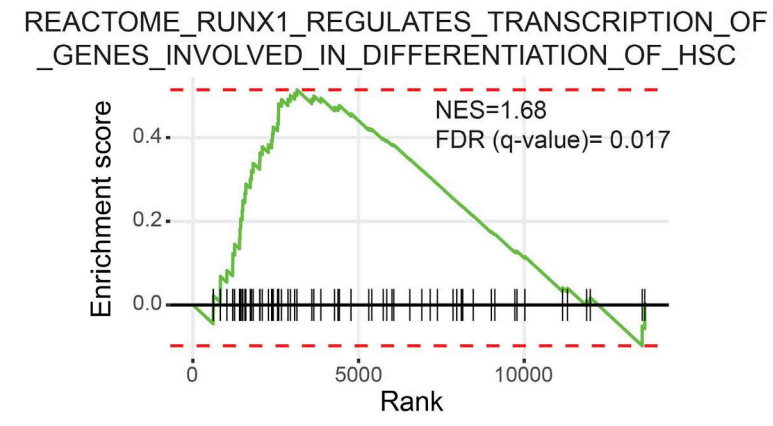

Figure 5. RUNX1 is a co-factor of NXK2-1. (A) Volcano plot showing differentially detected NKX2-1 binding proteins by immunoprecipitation-mass spectrometry (IP-MS) in NKX2-1$^{+/+}$ compared to NKX2-1$^{-/-}$ RPMI-8402 clones and IgG IP. Four clones per genotype were analyzed. The gray dotted lines indicate the cut-off values for significance (qvalue<0.1) and fold change (FC>2). (B) Immunoblot for NKX2-1, RUNX1 and histone 3 (H3) of input, IgG control and RUNX1 immunoprecipitated samples of NKX2-1$^{+/+}$ or NKX2-1$^{-/-}$ RPMI-8402 cells (mix of 4 clones per genotype) (left) or NKX2-1 positive patient derived xenograft (PDX) XB14 sample (right). (C) iRegulon analysis on significantly differentially expressed genes (DEG) in NKX2-1$^{+/+}$ RPMI-8402 clones compared to NKX2-1$^{-/-}$ clones. NKX6-3 was identified as top-scoring motif for the NKX family but has high similarity to NKX2-1. Normalized enrichment score (NES) values for each cluster code are shown from each transcription factor. DEG are colored according to their logFC. (D) Representative motifs from two top-scoring motif families, ranked on *P* value, identified by HOMER motif enrichment analysis on NKX2-1 chromatin immunoprecipitation-sequencing (ChIP-seq) from NKX2-1$^{+/+}$ clones. (E) iRegulon analysis on top 10% significantly DEG in NKX2-1-positive compared to NKX2-1-negative T-ALL samples (patient data from Pölönen *et al.*[16]). Predicted transcription factors are indicated in orange and blue octagons. NES values for each cluster code are shown for each transcription factor. DEG are colored according to their logFC. (F) GSEA enrichment plot showing upregulation of RUNX1-regulated genes involved in hematopoietic stem cell (HSC) differentiation in NKX2-1-positive T-ALL (patient data from Pölönen *et al.*[16]).

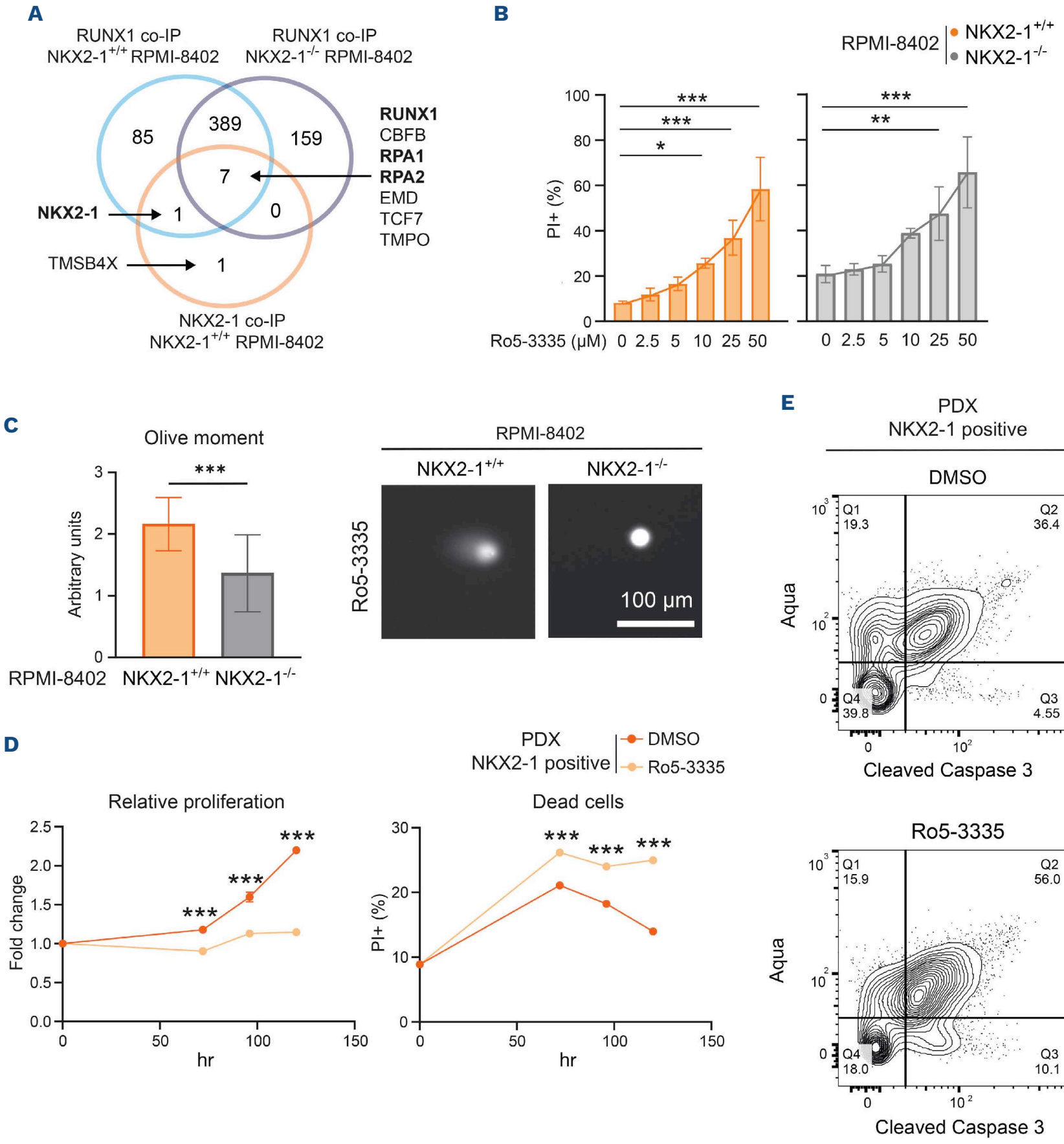

Continued on following page.

Figure 6. NKX2-1 alters RUNX1 binding partners and modulates sensitivity to RUNX1 inhibition. (A) Venn diagram illustrating significantly bound proteins to RUNX1 in NKX2-1$^{+/+}$ (light blue) or NKX2-1$^{-/-}$ (purple) RPMI-8402 clones and to NKX2-1 in NKX2-1$^{+/+}$ clones (orange). (B) Percentage of propidium iodide (PI)-positive dead cells detected by flow cytometry in NKX2-1$^{+/+}$ and NKX2-1$^{-/-}$ RPMI-8402 cells after treatment with Ro5-3335 for five days. Data represented as mean ± Standard Deviation (SD). Statistics calculated by an ordinary one-way ANOVA followed by a Tukey's HSD post hoc test. (C) (Left) Olive moment measured in comet assays on NKX2-1$^{+/+}$ and NKX2-1$^{-/-}$ RPMI-8402 cells after five days of treatment with 50 μM Ro5-3335. Data represented as mean ± Standard Error of Mean (SEM). Statistics calculated by Mann-Whitney two-tailed test. (Right) Representative comet stained with PI from NKX2-1$^{+/+}$ and NKX2-1$^{-/-}$ RPMI-8402 cells after five days of treatment with 50 μM Ro5-3335. (D) Effect of treatment of NKX2-1-positive patient derived xenograft (PDX) XB41 with 50 μM Ro5-3335 or DMSO vehicle. (Left) Relative proliferation of treated cells normalized to day 0. (Right) Absolute percentage of dead cells, identified as PI-positive cells by flow cytometry. Individual dots represent 3 technical replicates. Data represented as mean ± SD. Statistics calculated by two-way ANOVA followed by a Šidák test. (E) Flow cytometry analysis of cleaved caspase 3/Zombie Aqua of XB47 NKX2-1 positive PDX cells after 72 hours (hr) of treatment with DMSO vehicle or 50 μM Ro5-3335. (F) Proposed model of the role of NKX2-1 in T-ALL (Created with Servier Medical Art released under the Creative Commons Attribution 4.0 International License). *P<0.05, **P<0.01, ***P<0.001. P values were calculated using a two-tailed t test.

NKX2-1 reduced apoptotic cell death over time, suggesting that NKX2-1 plays a role in supporting cell survival. In RPMI-8402 cells, we previously showed that NKX2-1 knockout increases ROS levels,[15] which may explain better survival of NKX2-1 positive cells. Our results are consistent with previous studies, which showed that NKX2-1 knockdown increases expression of apoptosis-related genes in LUAD and promotes apoptosis in small-cell lung cancer and neuroblasts.[34-36] However, other research has demonstrated that NKX2-1 can induce cell death through apoptosis in thyroid carcinoma cells.[37] This aligns with the previously suggested idea of NKX2-1 being a double-edged sword, supporting the notion that its effects may vary depending on the genetic context in which it is expressed.[10]

To decipher the chromatin binding areas of NKX2-1, we performed ChIP-seq on our RPMI-8402 model. Among the 496 detected peaks, one of them was in *CDK6*. Our data support the view that NKX2-1 regulates CDK6 at the transcriptional level. Interestingly, the same *CDK6* region where NKX2-1 binding takes place coincided with a RUNX1 binding site (Figure 2B). Furthermore, our dual-luciferase reporter assays show that NKX2-1 and RUNX1 work together to modulate the activity of this CDK6 regulatory region (*Online Supplementary Figure S5*), further underscoring the idea of RUNX1 and NKX2-1 being essential co-factors for transcriptional regulation in T-ALL. Previous studies have shown that NKX2-1 also inhibits CDK6 transcription in LUAD.[38] The observed CDK6 regulation by NKX2-1 may explain the reduction in cell cycle progression that we observed in NKX2-1$^{+/+}$ clones. However, this regulation of CDK6 may also have indirect consequences for regulating the metabolism of NKX2-1 cells. Indeed, whereas we previously showed that NKX2-1 binds and transcriptionally induces the *de novo* serine and glycine synthesis pathway in T-ALL,[15] cyclin D3:CDK4/6 complex has also been identified as an indirect regulator of *de novo* serine and glycine synthesis in T-ALL.[39] Thus, our findings support the idea that NKX2-1 directly regulates CDK6 expression, driving cell cycle dysregulation, and potentially also contributing to the NKX2-1-dependent induction of *de novo* serine/glycine synthesis addiction in T-ALL.

Further unraveling the role of NKX2-1 in T-ALL, GSEA on our RNA-seq data in the RPMI-8402 model identified three interesting clusters of enriched gene sets regulated by NKX2-1, including ribosomal gene sets. However, these detected transcriptional changes did not result in strong ribosomal phenotypes in the polysome profile or global protein synthesis. However, NKX2-1 knockout may modulate ribosomal function in a milder fashion, by leading to specialized ribosomes with more subtle altered translation phenotypes, such as has been described for the RPL10 R98S mutation.[40,41] Furthermore, knocking out NKX2-1 may impact the extra-ribosomal functions of ribosomal proteins, which have been associated with tumorigenesis.[42,43] Interestingly, Liu *et al*. previously showed that mutations in ribosomal protein genes are highly enriched in cases of NKX2-1 overexpression, suggesting a potential synergy.[26]

Another gene set cluster that was enriched in our NKX2-1 model was linked to epigenetics, confirmed by a differential amount of histone marks. Intriguingly, all the histone modifications that were checked (both activating marks H3K27ac, H3K4me3 and H3K4me1, as well as repressive marks like H3K27me3) were strongly down-regulated in the presence of NKX2-1. In line with this, NKX2-1 did not act purely as a repressor or as an activator, and NKX2-1 ChIP-seq targets were induced or repressed (*Online Supplementary Figure S4*). Interestingly, *HDAC4* was identified as a gene whose promoter region is bound by NKX2-1, resulting in transcriptional upregulation in NKX2-1$^{+/+}$ cells. This may explain the detected differences in histone acetylation. Furthermore, we previously showed that NKX2-1 regulates chromatin DNA and histone demethylases by modifying the ratio between succinate and alpha-ketoglutarate in lung cancer, which function as co-substrate of various histone demethylase enzymes.[15,44] From a therapeutic perspective, the down-regulated histone marks in NKX2-1-driven T-ALL were associated with decreased sensitivity for HDACi like romidepsin and vorinostat, both clinically approved drugs that have been investigated for treatment of T-ALL.[45-48]

Our observations related to the function of NKX2-1 to protect against DNA damage also have clinical relevance. Etoposide, doxorubicin and 6-TG are clinically used DNA-damaging agents to which NKX2-1-expressing cells showed reduced sensitivity.[49-51] NKX2-1 presence was associated with lower levels of γ-H2AX and reduced apoptosis, suggesting a role in

minimizing DNA damage and promoting cell survival. Interestingly, we also found that NKX2-1 binds to RPA1 and RPA2, proteins involved in DNA damage repair.[30] A role of NKX2-1 in DNA damage was already reported, as its overexpression was found to protect cells from DNA damage from DNA replication stress in LUAD by its binding with DDB1, a DNA damage response sensor protein found in UV-induced DNA lesions, and to RPA32.[52] In the context of LUAD and T-ALL, we also showed that NKX2-1 lowers ROS levels,[15] which may also add to the protective role of NKX2-1 against DNA damage.

Based on the NKX2-1 IP-MS results, we discovered that the transcription factor RUNX1 is a co-factor of NKX2-1. In addition to physical binding of these two proteins, our data also support a co-operative role in transcriptional regulation. HOMER motif analysis on the NKX2-1 ChIP-seq peaks identified RUNX1 motifs among the top-scoring motifs, and regulatory transcriptional network analysis on DEG from RNA-seq of our RPMI-8402 model and from T-ALL patient data also showed RUNX1 as a top upstream transcription factor together with NKX family members, confirming a tight co-operation between these factors.

Given its different roles during hematopoiesis, RUNX1 is known to interact with other transcription factors and to recruit various co-factors to the chromatin. In this way, RUNX1 modifies the chromatin landscape and the transcriptional activity of its target genes. RUNX1 has been demonstrated to form a core transcriptional regulatory circuit in T-ALL with TAL1 and GATA3, as well as TLX1 and STAT5.[28,53] Here, we show that also NKX2-1 is one of the co-factors that co-operates with RUNX1, co-regulating expression of gene sets crucial for T-ALL tumorigenesis.[22] Additionally, the greater sensitivity of NKX2-1$^{+/+}$ clones to RUNX1 inhibition reinforces the importance of NKX2-1 in supporting the cellular mechanisms orchestrated by RUNX1, thus emphasizing their interdependent roles in T-ALL progression. Given the importance of RUNX1 in hematopoiesis, and its known functions independent of NKX2-1, it is not surprising that also NKX2-1 negative T-ALL cell lines display RUNX1 inhibitor sensitivity (*Online Supplementary Figure S21*), and targeting of RUNX1 for therapeutic purposes may have a limited therapeutic window.

In conclusion, the findings in this study (summarized in Figure 6F) highlight the critical role of NKX2-1 in regulating T-ALL maturation state, protecting cells from apoptosis and altering their cell cycle progression. Moreover, NKX2-1 confers resistance to DNA damage and HDACi. We analyzed the binding partners of NKX2-1 and found a novel tight relationship with RUNX1 in co-operatively driving the T-ALL transcriptional network.

Disclosures

No conflicts of interest to disclose.

Contributions

LVA, KT, KDK and DCG are responsible for study concept and design; LVA, KT, DDG, EH, PV, MC, LL, AV, JR, JV and DCG are responsible for data collection; LVA, SD, KT, MC, DP, NB, HS, KRK, JC, KDK and DCG are responsible for data analysis and interpretation; LVA, KDK and DCG drafted the article; DCG and KDK jointly supervised this work and approved the final version of the manuscript for publication. All authors critically reviewed the article.

Acknowledgments

We thank the KU Leuven Genomics, FACS and flow cytometry and Bioimaging Leuven Core Facilities as well as our collaborators from Proteomics Leuven – Laboratory of Applied Mass Spectrometry (LAMaS) for their contribution to this work. For the analysis of RNA- and ChIP-sequencing samples, resources and services provided by the VSC (Flemish Supercomputer Center), funded by the Research Foundation – Flanders (FWO) and the Flemish Government, were used. We thank the lab of Tom Taghon for kindly providing the OP9-hDLL4 cells used in this study, the lab of Geert Mortier for the RUNX1 overexpression plasmid, and Óscar Herranz for thorough proofreading of the manuscript.

Funding

This research was funded by grants from KU Leuven (C14/18/104), iBOF (iBOF/23/014), Kom op tegen Kanker (Emmanuel Van Der Schueren), Fonds Wetenschappelijk Onderzoek (FWO) (G0A4220N, G092620N) and by fundraising initiatives from VZW Baief. EH and PV received an FWO PhD fellowship fundamental research grant (1106121N and 1116822N), and AV was supported by a postdoctoral fellowship from FWO (12AZ324N).

Data-sharing statement

Data generated in this study are available within the article and its Online Supplementary Appendix. RNA-sequencing and ChIP-seq data are available on Gene Expression Omnibus (GEO) with accession numbers GSE288187 and GSE288188. Mass spectrometry data are available in PRIDE with identifiers PXD057622 and PXD057654.

References

1. Girardi T, Vicente C, Cools J, De Keersmaecker K. The genetics and molecular biology of T-ALL. Blood. 2017;129(9):1113-1123.
2. De Keersmaecker K, Atak ZK, Li N, et al. Exome sequencing identifies mutation in CNOT3 and ribosomal genes RPL5 and RPL10 in T-cell acute lymphoblastic leukemia. Nat Genet. 2013;45(2):186-190.
3. Tran TH, Hunger SP. The genomic landscape of pediatric acute lymphoblastic leukemia and precision medicine opportunities.

Semin Cancer Biol. 2022;84:144-152.
4. Brady SW, Roberts KG, Gu Z, et al. The genomic landscape of pediatric acute lymphoblastic leukemia. Nat Genet. 2022;54(9):1376-1389.
5. Homminga I, Pieters R, Langerak AW, et al. Integrated transcript and genome analyses reveal NKX2-1 and MEF2C as potential oncogenes in T cell acute lymphoblastic leukemia. Cancer Cell. 2011;19(4):484-497.
6. Lazzaro D, Price M, de Felice M, Di Lauro R. The transcription factor TTF-1 is expressed at the onset of thyroid and lung morphogenesis and in restricted regions of the foetal brain. Development. 1991;113(4):1093-1104.
7. Willemsen MAAP, Breedveld GJ, Wouda S, et al. Brain-thyroid-lung syndrome: a patient with a severe multi-system disorder due to a de novo mutation in the thyroid transcription factor 1 gene. Eur J Pediatr. 2005;164(1):28-30.
8. Weir BA, Woo MS, Getz G, et al. Characterizing the cancer genome in lung adenocarcinoma. Nature. 2007;450(7171):893-898.
9. Yamaguchi T, Hosono Y, Yanagisawa K, Takahashi T. NKX2-1/TTF-1: an enigmatic oncogene that functions as a double-edged sword for cancer cell survival and progression. Cancer Cell. 2013;23(6):718-723.
10. Yamaguchi T, Yanagisawa K, Sugiyama R, et al. NKX2-1/TITF1/TTF-1-induced ROR1 is required to sustain EGFR survival signaling in lung adenocarcinoma. Cancer Cell. 2012;21(3):348-361.
11. Watanabe H, Francis JM, Woo MS, et al. Integrated cistromic and expression analysis of amplified NKX2-1 in lung adenocarcinoma identifies LMO3 as a functional transcriptional target. Genes Dev. 2013;27(2):197-210.
12. Niimi T, Nagashima K, Ward JM, et al. claudin-18, a novel downstream target gene for the T/EBP/NKX2.1 homeodomain transcription factor, encodes lung- and stomach-specific isoforms through alternative splicing. Mol Cell Biol. 2001;21(21):7380-7390.
13. Baca SC, Takeda DY, Seo J-H, et al. Reprogramming of the FOXA1 cistrome in treatment-emergent neuroendocrine prostate cancer. Nat Commun. 2021;12(1):1979.
14. Ferrando AA, Neuberg DS, Staunton J, et al. Gene expression signatures define novel oncogenic pathways in T cell acute lymphoblastic leukemia. Cancer Cell. 2002;1(1):75-87.
15. Heylen E, Verstraete P, Van Aerschot L, et al. Transcription factor NKX2-1 drives serine and glycine synthesis addiction in cancer. Br J Cancer. 2023;128(10):1862-1878.
16. Pölönen P, Di Giacomo D, Seffernick AE, et al. The genomic basis of childhood T-lineage acute lymphoblastic leukaemia. Nature. 2024;632(8027):1082-1091.
17. Mootha VK, Lindgren CM, Eriksson K-F, et al. PGC-1α-responsive genes involved in oxidative phosphorylation are coordinately downregulated in human diabetes. Nat Genet. 2003;34(3):267-273.
18. Subramanian A, Tamayo P, Mootha VK, et al. Gene set enrichment analysis: a knowledge-based approach for interpreting genome-wide expression profiles. Proc Natl Acad Sci U S A. 2005;102(43):15545-15550.
19. Garrido-Martín D, Palumbo E, Guigó R, Breschi A. ggsashimi: Sashimi plot revised for browser- and annotation-independent splicing visualization. PLoS Comput Biol. 2018;14(8):e1006360.
20. Quentmeier H, Pommerenke C, Dirks WG, et al. The LL-100 panel: 100 cell lines for blood cancer studies. Sci Rep. 2019;9(1):114.
21. Kalender Atak Z, Gianfelici V, Hulselmans G, et al. Comprehensive analysis of transcriptome variation uncovers known and novel driver events in T-cell acute lymphoblastic leukemia. PLoS Genet. 2013;9(12):e1003997.
22. Sanda T. RUNX1 in T-ALL: tumor suppressive or oncogenic? Blood. 2017;130(15):1686-1688.
23. Rheinländer A, Schraven B, Bommhardt U. CD45 in human physiology and clinical medicine. Immunol Let. 2018;196:22-32.
24. Dawes R, Petrova S, Liu Z, Wraith D, Beverley PCL, Tchilian EZ. Combinations of CD45 isoforms are crucial for immune function and disease. J Immunol. 2006;176(6):3417-3425.
25. Morgan DO. Cyclin-dependent kinases: engines, clocks, and microprocessors. Annu Rev Cell Dev Biol. 1997;13(1):261-291.
26. Liu Y, Easton J, Shao Y, et al. The genomic landscape of pediatric and young adult T-lineage acute lymphoblastic leukemia. Nat Genet. 2017;49(8):1211-1218.
27. Choi Ah, Illendula A, Pulikkan JA, et al. RUNX1 is required for oncogenic Myb and Myc enhancer activity in T-cell acute lymphoblastic leukemia. Blood. 2017;130(15):1722-1733.
28. Sanda T, Lawton LN, Barrasa MI, et al. Core transcriptional regulatory circuit controlled by the TAL1 complex in human T cell acute lymphoblastic leukemia. Cancer Cell. 2012;22(2):209-221.
29. Della Gatta G, Palomero T, Perez-Garcia A, et al. Reverse engineering of TLX oncogenic transcriptional networks identifies RUNX1 as tumor suppressor in T-ALL. Nat Med. 2012;18(3):436-440.
30. He Z, Henricksen LA, Wold MS, Ingles CJ. RPA involvement in the damage-recognition and incision steps of nucleotide excision repair. Nature. 1995;374(6522):566-569.
31. Cunningham L, Finckbeiner S, Hyde RK, et al. Identification of benzodiazepine Ro5-3335 as an inhibitor of CBF leukemia through quantitative high throughput screen against RUNX1-CBFβ interaction. Proc Natl Acad Sci U S A. 2012;109(36):14592-14597.
32. Illendula A, Gilmour J, Grembecka J, et al. Small molecule inhibitor of CBFβ-RUNX binding for RUNX transcription factor driven cancers. EBioMedicine. 2016;8:117-131.
33. Preußner M, Schreiner S, Hung L-H, et al. HnRNP L and L-like cooperate in multiple-exon regulation of CD45 alternative splicing. Nucleic Acids Res. 2012;40(12):5666-5678.
34. Isogaya K, Koinuma D, Tsutsumi S, et al. A Smad3 and TTF-1/NKX2-1 complex regulates Smad4-independent gene expression. Cell Res. 2014;24(8):994-1008.
35. Kong R, Patel AS, Sato T, et al. Transcriptional circuitry of NKX2-1 and SOX1 defines an unrecognized lineage subtype of small-cell lung cancer. Am J Respir Crit Care Med. 2022;206(12):1480-1494.
36. Jia S, Zhang L, Zhang K, et al. Nkx2.1 downregulation is involved in brain abnormality induced by excess retinoic acid. Acta Biochim Biophys Sin (Shanghai). 2020;52(6):683-690.
37. Ito Y, Furuya F, Taki K, Suzuki H, Shimura H. NKX2-1 re-expression induces cell death through apoptosis and necrosis in dedifferentiated thyroid carcinoma cells. PLoS One. 2021;16(11):e0259558.
38. Maeda Y, Tsuchiya T, Hao H, et al. KrasG12D and Nkx2-1 haploinsufficiency induce mucinous adenocarcinoma of the lung. J Clin Invest. 2012;122(12):43884400.
39. Wang H, Nicolay BN, Chick JM, et al. The metabolic function of cyclin D3-CDK6 kinase in cancer cell survival. Nature. 2017;546(7658):426430.
40. Kampen KR, Fancello L, Girardi T, et al. Translatome analysis reveals altered serine and glycine metabolism in T-cell acute lymphoblastic leukemia cells. Nat Commun. 2019;10(1):2542.
41. Caruso M, De Keersmaecker K. Ribosome specialization by cancer-associated ribosomal protein mutations: progress made and open questions. Philo Trans R Soc Lond B Biol Sci. 2025;380(1921):20230380.
42. Sulima SO, Hofman IJF, De Keersmaecker K, Dinman JD. How ribosomes translate cancer. Cancer Discov. 2017;7(10):1069-1087.
43. Sulima SO, Kampen KR, Vereecke S, et al. Ribosomal lesions

promote oncogenic mutagenesis. Cancer Res. 2019;79(2):320-327.
44. Tran TQ, Lowman XH, Kong M. Molecular pathways: metabolic control of histone methylation and gene expression in cancer. Clin Cancer Res. 2017;23(15):4004-4009.
45. Brunvand MW, Carson J. Complete remission with romidepsin in a patient with T-cell acute lymphoblastic leukemia refractory to induction hyper-CVAD. Hematol Oncol. 2018;36(1):340-343.
46. Song Y, Chen S, Liu C, et al. Chemo-free maintenance therapy in adult T-cell acute lymphoblastic leukemia: a case report and literature review. Front Pharmacol. 2023;14:1051305.
47. Burke MJ, Lamba JK, Pounds S, et al. A therapeutic trial of decitabine and vorinostat in combination with chemotherapy for relapsed/refractory acute lymphoblastic leukemia. Am J Hematol. 2014;89(9):889-895.
48. Burke MJ, Kostadinov R, Sposto R, et al. Decitabine and vorinostat with chemotherapy in relapsed pediatric acute lymphoblastic leukemia: a TACL pilot study. Clin Cancer Res. 2020;26(10):2297-2307.
49. Whitlock JA, Malvar J, Dalla-Pozza L, et al. Nelarabine, etoposide, and cyclophosphamide in relapsed pediatric T-acute lymphoblastic leukemia and T-lymphoblastic lymphoma (study T2008-002 NECTAR). Pediatr Blood Cancer. 2022;69(11):e29901.
50. Escherich G, Zimmermann M, Janka-Schaub G. Doxorubicin or daunorubicin given upfront in a therapeutic window are equally effective in children with newly diagnosed acute lymphoblastic leukemia. A randomized comparison in trial CoALL 07-03. Pediatr Blood Cancer. 2013;60(2):254-257.
51. Toksvang LN, Als-Nielsen B, Bacon C, et al. Thiopurine enhanced ALL maintenance (TEAM): study protocol for a randomized study to evaluate the improvement in disease-free survival by adding very low dose 6-thioguanine to 6-mercaptopurine/methotrexate-based maintenance therapy in pediatric and adult patients (0-45 years) with newly diagnosed B-cell precursor or T-cell acute lymphoblastic leukemia treated according to the intermediate risk-high group of the ALLTogether1 protocol. BMC Cancer. 2022;22(1):483.
52. Liu Z, Yanagisawa K, Griesing S, et al. TTF-1/NKX2-1 binds to DDB1 and confers replication stress resistance to lung adenocarcinomas. Oncogene. 2017;36(26):3740-3748.
53. Vanden Bempt M, Demeyer S, Broux M, et al. Cooperative enhancer activation by TLX1 and STAT5 drives development of NUP214-ABL1/TLX1-positive T cell acute lymphoblastic leukemia. Cancer Cell. 2018;34(2):271-285.e7.